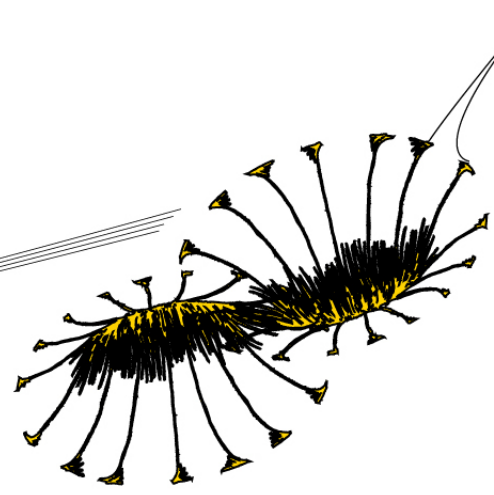


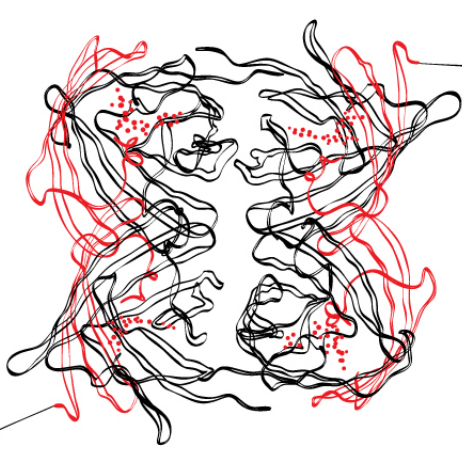


Self-Assembly of Nanowires



Joren van Kempen

*Inorganic Materials Science Group,
Faculty of Science & Technology,
University of Twente*



August 13, 2013

Abstract

Self-assembly of Au and Ag|ZnO nanowires, synthesized by templated electrodeposition, was studied by making use of thiol-functionalized silica nanoparticles with a maghemite core (SiMAG) or by using thiol-modified complimentary DNA oligomers. Self-assembly samples were studied by scanning electron microscopy (SEM) and Dynamic Light Scattering (DLS). SEM and DLS both indicated the possibility of successful self-assembly when using SiMAG nanoparticles to induce self-assembly. The effect of time and of nanowire and SiMAG nanoparticle concentration was examined as well.

Contents

Introduction	8
1 Theory	9
1.1 Nanostructured Materials	9
1.2 Self-Assembly	10
1.3 Templated Electrodeposition	15
2 Materials and Methods	19
2.1 Membrane Preparation	19
2.2 Nanowire Synthesis	19
2.3 Self-Assembly Sample Preparation	20
2.3.1 SiMAG Sample Preparation	21
2.3.2 Oligomer Sample Preparation	22
2.3.3 Sample Examination	23
3 Results and Discussion	25
3.1 Self-Assembly of Nanowires with SiMAG nanoparticles	25
3.1.1 Freeze-Drying	26
3.1.2 The Effect of Self-Assembly Time	27
3.1.3 The Effect of SiMAG nanoparticle concentration	28
3.1.4 Self-Assembly Studied by DLS	28
3.2 Self-Assembly of Nanowires with DNA Oligomers	33
Conclusions and Recommendations	35
Acknowledgments	37
References	39

Introduction

Nanotechnology is one of the most promising fields of research today. It is expected to have enormous societal and economic impact in the near future. Current nanometer-scale technology, such as carbon nanotubes or the ever-increasing number of transistors on one chip, already point to this. Materials research on the nanometer scale is a large part of nanotechnology. Understanding how the properties of materials arise, and more importantly, how to manipulate or achieve desired properties is fundamental in this regard. For applications, zero-dimensional (0D) structures all the way up to complex three-dimensional (3D) structures, often made up of lower dimensional structures, are all of interest. These structures can be tailored to specific requirements and to exhibit desired properties. Nanowires (as well as nanotubes and nanorods) are one-dimensional (1D) structures that can be one of the building blocks for larger dimensional structures. These 1D objects have unique electronic, thermal and mechanical properties, mainly in the direction of the long axis. Harnessing these properties would allow for many possible applications in electronic, optoelectronic and electrochemical devices. Furthermore, 1D structures are of interest because of the wide variety of possible synthesis techniques. Some of these are also cheap and well-suited for upscaling, making them possible candidates for commercial applications. One of these promising techniques is templated electrodeposition.

To actually create 2D or 3D structures from 1D structures, self-assembly is often used. There are many possible self-assembly techniques available, giving researchers a lot of flexibility in their approach. Some of these techniques rely on gravitational or electric forces, while others rely on (bio)chemical processes making use of surfactants or biomolecules. In this study, the focus is on the chemical side of self-assembly. SiMAG nanoparticles provide a means to attach soft metal nanowires, such as Ag, Au, or Pt, to them by thiol groups attached to the silica shell. Besides these nanoparticles, complementary DNA oligomers, also functionalized with thiol groups, were also used to attempt to link nanowires by complementary base pair sequences.

Using the previously introduced techniques, Ag|ZnO or Au nanowires were synthesized to use in self-assembly experiments. These experiments consisted of using SiMAG-Thiol nanoparticles or complementary DNA oligomers to induce self-assembly. This thesis starts with a theoretical section on the main concepts of this study. It continues with the experimental section, where the experimental procedures are explained. Finally, the results of these experiments are discussed and conclusions are drawn. Some recommendations are also given for possible continuation of this study.

The main goal of this study is to show self-assembly of nanowires with either SiMAG nanoparticles or DNA oligomers. This goal will be achieved if it can be conclusively shown

that either of these combinations reproducibly induce self-assembly and is not the result of some other uncontrollable effect. In this case, self-assembly means the formation of an arbitrary shaped cluster containing nanowires that sustains its form despite external influences. To accomplish this goal, two research questions were devised to aid in the understanding of self-assembly:

1. How can we induce self-assembly between nanowires and nanoparticles, or between multiple nanowires of a different kind?
2. What are the main parameters that influence self-assembly of nanowires and nanoparticles?

Chapter 1

Theory

Various techniques were used during this research, namely radio frequency sputtering, templated electrodeposition, self-assembly, and analysis by dynamic light scattering and scanning electron microscopy. The following chapter describes the basic principles behind some of these techniques.

1.1 Nanostructured Materials

Nanostructured materials have become one of the top research fields of interest in nanotechnology and materials science. When reading the term nanostructured materials, two ideas generally come to mind. One is that something of interest occurs at the nanometer scale and deserves study, and the second is that there is some level of human control possible at the nanometer scale in either synthesizing or ordering a material. Both these ideas lie at the heart of materials science: to understand the composition and structure of a material and its relation to the material's properties, and being able to use that knowledge to synthesize materials for a wide variety of applications. However, there are more reasons why nanostructured materials are so interesting. They encompass most materials, since almost all material properties depend on some feature at the nanometer scale. Furthermore, new properties arise at this scale, e.g., the increased stiffness and electrical conductivity of buckyballs, and the wide range of fluorescent emissions of CdSe quantum dots. A lot of these new properties arise from the fact that classical and quantum behavior are no longer necessarily separated for these materials and are able to mix. Finally, nanostructured materials allow for a bridge between the classical and the biological sciences [1]. Well-known examples are Lab-on-a-chip devices that could be implanted in the body to measure parameters like temperature or blood oxygen levels.

As mentioned before, the term nanostructured materials implies some form of control in synthesis or ordering of the material. There are two main synthesis approaches, top-down and bottom-up. The top-down approach is generally a destructive technique, as a bulk material is decomposed in a controlled fashion to create a desired structure. This approach is prevalent in the chip industry, where lithography is used to etch channels and other structures in Si wafers. This approach allows for long range order (on the nanometer scale), however there is a limit to precision and to how small structures can become. It is also often a

2D technique in which material is etched away layer-by-layer, leaving a structure instead. This adds extra difficulty to the synthesis, since more thought has to go into the etching procedure. The bottom-up approach makes use of atoms and molecules as building blocks to create desired structures. Structures synthesized this way are often made in parallel and nearly identical to one another. Depending on the technique used, it is also possible to make large quantities of the structure in a single synthesis. However, long range order is only possible when incorporating these structures into larger materials [1]. An example of a bottom-up synthesis is templated electrodeposition, as will be explained in section 1.3.

1.2 Self-Assembly

Self-assembly can be used to overcome the downsides of the two approaches. Self-assembly is the term used for the process of organizing a disordered system without external direction, by making use of, e.g., the lowest energy configuration of the components of the system. Self-assembly is a bottom-up approach at its core. Self-assembly allows bottom-up synthesized nanostructures to organize themselves in regular patterns, often applied by a top-down approach, by making use of local forces to find the lowest energy configuration [1]. In this regard self-assembly can be seen as a bridge between top-down and bottom-up approaches. This also makes self-assembly a very important tool when dealing with nanostructured materials. Self-assembled monolayers (SAMs) are a well-known example hereof and topic of much research interest [2][3][4].

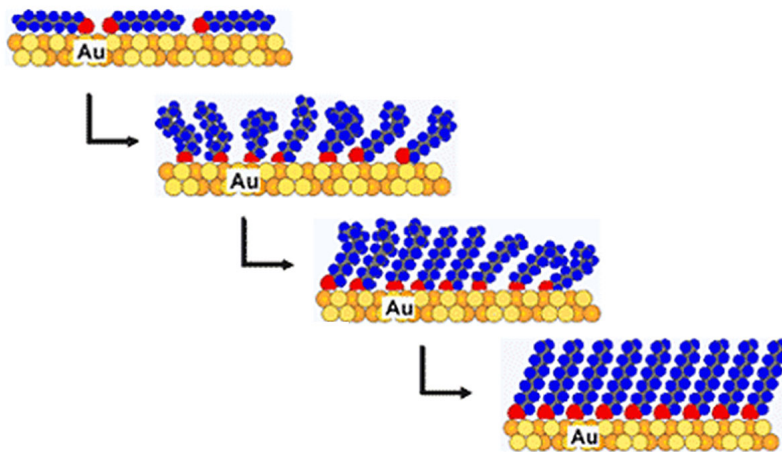


Figure 1.1: Schematic representation of a self-assembled monolayer of alkanethiolates forming on a Au surface [5].

Self-assembly using nanowires and nanorods is also a field of interest [6]. These 1D nanostructures are of interest because they often have enhanced electrical and/or thermal transport properties. To harness these properties, self-assembly mechanisms are often required to achieve order. Since nanowires are anisotropic in terms of shape compared to for example 0D nanostructures (e.g. quantum dots), there are multiple self-assembled orientations possible. The challenge is therefore not only to achieve self-assembly, but also to

have the nanowires assemble in the desired orientation. Numerous techniques have been devised over the years to achieve self-assembly of nanowires, nanorods or nanotubes:

- **Electric field-assisted self-assembly:** an electric field is applied to a solution of nanorods containing a dipole moment. The field forces the nanowires into one orientation after which the solution is dried, leaving the nanorods in an ordered state, as shown in Figure 1.2 [7].

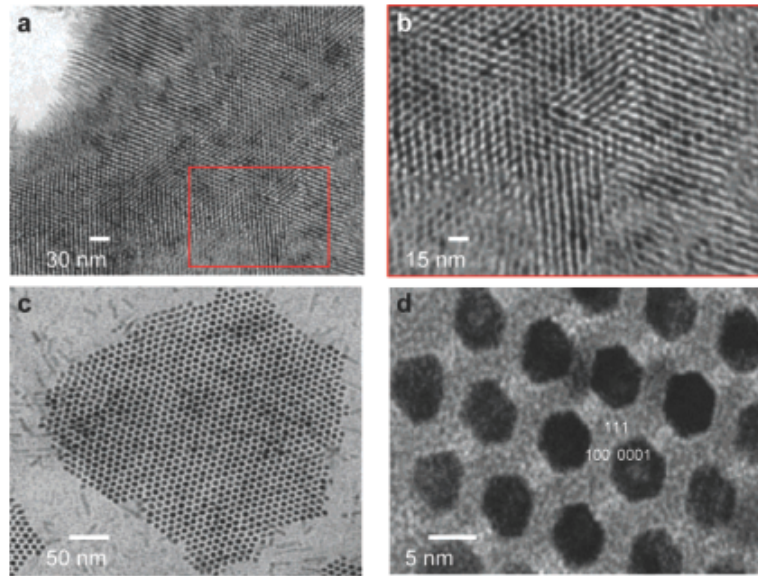


Figure 1.2: TEM image of perpendicularly aligned nanorod superlattices. (a) Section of CdS nanorod domain in absence of electric field. (b) Magnified section of (a), showing parallel to perpendicular alignment from edge to center. (c) CdS nanorod alignment under a field of $1 \text{ V}/\mu\text{m}$. (d) Azimuthal alignment of nanorods.

- **Templated self-assembly:** a template is used to force nanorods into a predefined superstructure mold, as shown in Figure 1.3. Once fixed, the template can be removed, leaving the nanorod superstructure [8]. The main advantage of this technique is the fact that it does not depend on a material's properties.

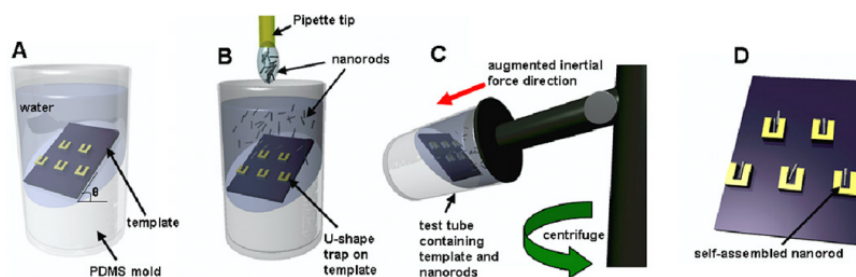


Figure 1.3: Templated self-assembly process scheme.

- **Gravity driven self-assembly:** nanotubes can be synthesized with large differences in density at the ends. When put in a solution, this causes the nanotubes to form a vertical structure [9]. A schematic representation of this process can be seen in Figure 1.4

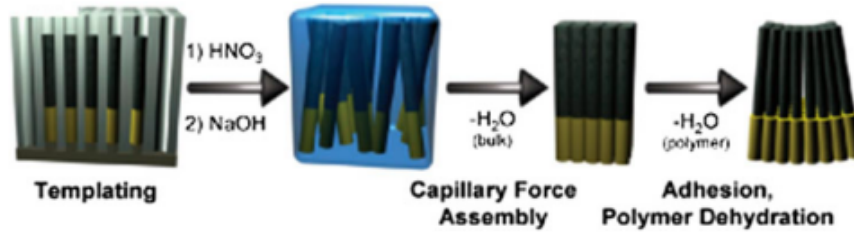


Figure 1.4: Gravity driven self-assembly process scheme.

- **Surfactant and chemically assisted self-assembly:** the core principle of this technique is to use the preferential binding of an active group to a material. Surfactants can be attached to certain faces of nanorods. This either shields these faces, forcing self-assembly at the exposed faces, or the surfactants are used directly by manipulating the environment of the solution they are in, eliciting an effect from the surfactant, which then leads to self-assembly. An example of this makes use of cationic surfactant molecules attached to nanorods. By changing the pH, electrostatic interaction between the cationic surfactant bilayer around the nanorods and negatively charged self-assembled monolayers occurs, yielding a 2D superstructure [10]. Figure 1.5 shows a schematic representation of this effect. Another option, and one used in this study, is to use thiol groups, which have a strong affinity for soft metals like Au, Ag and Pt. These groups can be used as linkers to connect nanowires to each other.

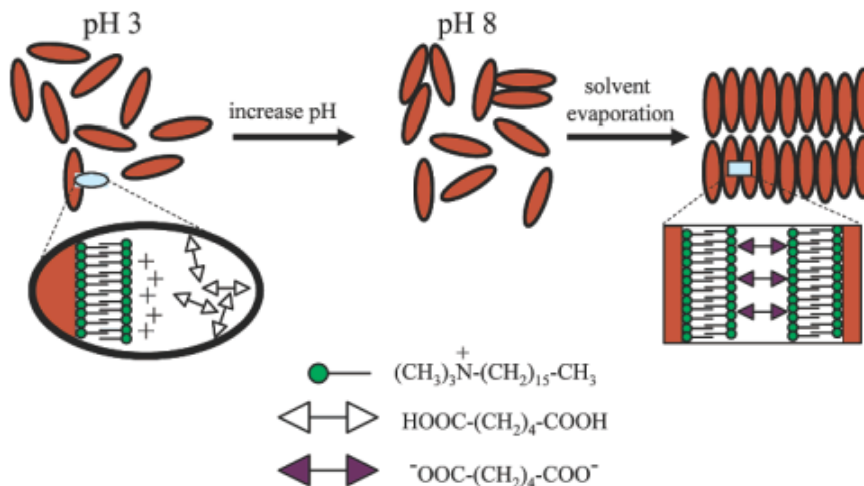


Figure 1.5: Scheme of the pH-directed assembly of gold nanorods using adipic acid that shows isolated, disordered nanorods at pH 3 and side-to-side assembled nanorods at pH 8.

- Biomolecular-assisted self-assembly:** this technique is very similar to the previous one. Often biomolecules are bound to nanorods and then left to link together. Complementary, thiolated oligonucleotides, which are basically short strings of single Watson-Crick bases with a thiol group at one end, can be used to facilitate this linking [11]. Alternatively, certain facets of nanorods can be covered by biomolecules, leaving other facets open for self-assembly in the right conditions [12]. Two very popular molecules in this self-assembly technique are biotin and streptavidin, due to their high binding affinity. Figure 1.6 shows yet another technique, where a biomolecular recognition system is used to form end-to-end assembled nanorods. Here, an antigen-antibody recognition system is used in the form of anti-mouse IgG, which provides an anchoring site at the end of a nanorod and interacts with mouse IgG for assembly [13].

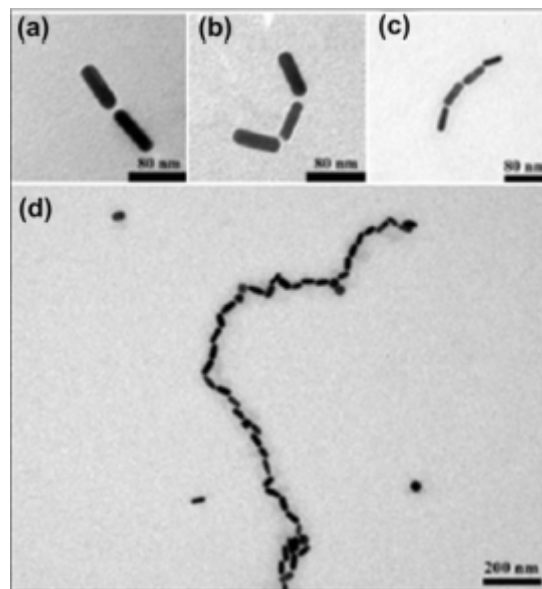


Figure 1.6: TEM images of (a) di-, (b) tri-, and (c) tetra-gold nanorods assembly. (d) Gold nanorods were assembled into successive chains via increasing the concentration of mouse IgG in a stepwise fashion.

- Langmuir-Blodgett self-assembly:** a thin film of nanorods is created at the water/air interface of a solution. This layer is then transferred directly onto a solid substrate by immersing/emersing it in/out of the solution, maintaining the order of the film [14]. TEM images of various stages of this process are shown in Figure 1.7.
- Solution phase self-assembly:** this technique makes use of depletion forces present between nanorods in solution to achieve order [15]. Concentration and solution contents greatly influence this technique. Figure 1.8 shows a schematic representation of this mechanism.

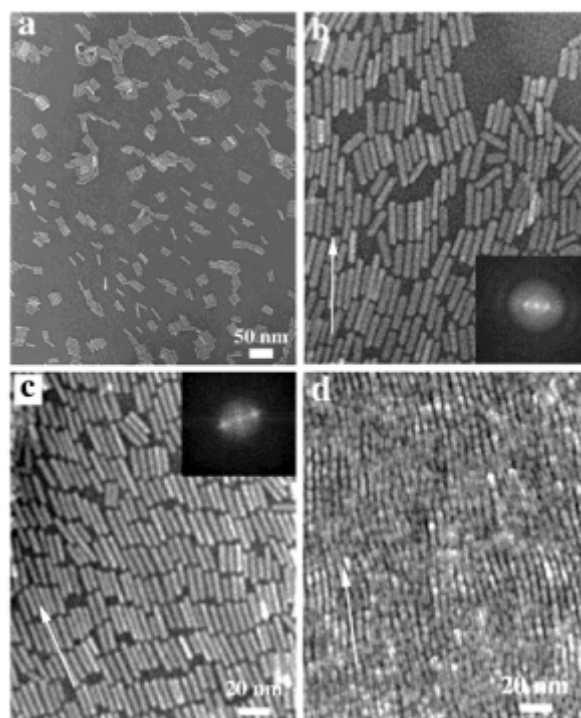


Figure 1.7: TEM images of nanorod assemblies at the water/air interface at different stages of compression: (a) isotropic distribution at low pressure; (b) monolayer with partial nematic arrangement; (c) monolayer with smectic arrangement; and (d) nanorod multilayer with nematic configuration. Insets in panels (b) and (c) are the Fourier transform of the corresponding image.

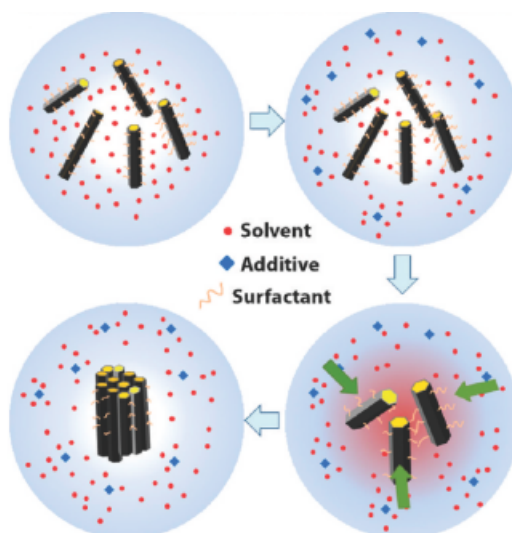


Figure 1.8: Schematic of solution phase self-assembly.

- **Solvent evaporation self-assembly:** similar to the previous method, nanorods are in solution. However, the solvent is allowed to evaporate for self-assembly. Often a grid or

other type of template is used either in the solution or as a place to put the solution on. As the solvent evaporates, nanorods are forced into increasingly small areas and start ordering themselves along the grid or template [16]. A schematic representation of this is shown in Figure 1.9.

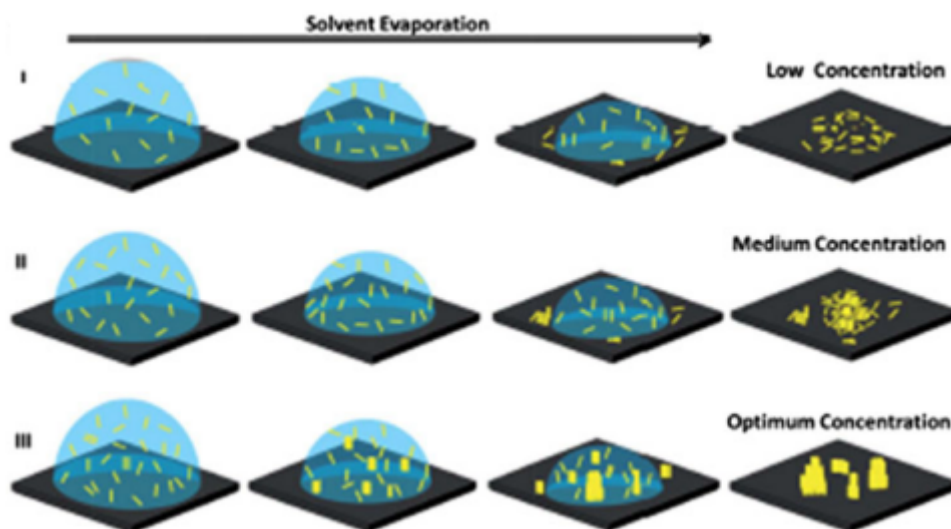


Figure 1.9: Schematic representation showing the progression of the nanorod assembly in different stages of droplet drying for different concentrations.

Two self-assembly mechanisms were examined in this study. One makes use of the preferential binding of noble metals with thiol groups, while the other makes use of complementary DNA oligomers, functionalized with thiol groups to be able to attach them to nanowires. These two methods were chosen for a number of reasons. Firstly, they are relatively easy to implement with the nanowires synthesis method used. On top of this, both induce self-assembly in a similar way, making sample preparation, handling and examination easier. Additionally, the underlying principle can be understood intuitively, making it a good choice for initial exploratory research. Finally, the superparamagnetic behavior of the nanoparticles would allow for further manipulation of the nanowires after self-assembly, such as providing an easy means of extracting the nanowires from solution.

1.3 Templated Electrodeposition

There are various techniques available for the synthesis of nanowires. Some of these are chemical vapor deposition, high-temperature catalytic processes, evaporation of mixed powder, molecular beam epitaxy and wet-chemical synthesis. Templated electrodeposition belongs to the latter category. It is a process that can operate at room temperature and ambient pressures, and uses relatively cheap and easy-to-use material sources. Additionally, it has a high throughput and high yields. On top of this, the process has a large freedom in regard to the composition of the resulting nanowires. Nanowires of a wide variety of material can be synthesized, as well as nanowires consisting of segments of different materials. This

makes templated electrodeposition an ideal technique when taking possible commercial application into account, besides research interests [17].

Electrodeposition makes use of an electrochemical cell, which consists of three electrodes immersed in an electrolyte. One of these electrodes is called the working electrode, which is where the actual deposition takes place. The function of another electrode, called the counter electrode, is to complete the electrochemical cell. Both electrodes are usually a noble metal, so they do not influence the deposition. In addition to the two functional electrodes, a reference electrode, with respect to which the potentials are measured, is often used. The reference electrode is made of phases with a constant composition. The internationally accepted primary reference is the normal hydrogen electrode (NHE), which has all components at unit activity. It is comprised of $\text{Pt}/\text{H}_2(a = 1)/\text{H}^+(a = 1, \text{aqueous})$. In this notation, the dashes represent a phase boundary. However, there are other common reference electrodes in use besides the normal hydrogen electrode. Two examples are the saturated calomel electrode, which is $\text{Hg}/\text{Hg}_2\text{Cl}_2/\text{KCl}$ (saturated in water), with a potential of 0.242 V vs. NHE and the silver-silver chloride electrode, which is $\text{Ag}/\text{AgCl}/\text{KCl}$ (saturated in water), with a potential of 0.197 V vs. NHE [18]. It should be noted that both reference potentials were measured at 25°C and at pH 0. Variations can occur depending on the concentration of the KCl filling solution.

To drive a deposition, a potential is applied to the working electrode with respect to the reference electrode. Diffusion causes ions to drift to the electrodes, where they react. In the meantime, electrons flow from the counter electrode to the working electrode to compensate the charge build-up. Because the ions are removed from the electrolyte solution, a gradient is formed, which becomes the driving force of the diffusion. Figure 1.10 shows this process schematically for a templated deposition onto a working electrode. Since different electrolytes contain different ions, different potentials are required for each electrolyte to drive the deposition. At the working electrode, a reduction reaction takes place to form solid material, while an oxidation reaction occurs at the counter electrode. Reaction (1.1) shows the general equation of a reduction reaction, where M^{n+} represents the metal ions in solution, n represents the number of electrons required for the reaction to proceed and M represents the solid material formed at the electrode. Because an external potential has to be applied to the cell to activate it, this kind of electrochemical cell is called an electrolytic cell [18].



When a template is applied over the working electrode, the metal ions are restricted in their freedom to reach the working electrode. The ions will form solid material in the template, following its structure. In this way, a variety of structures can be synthesized.

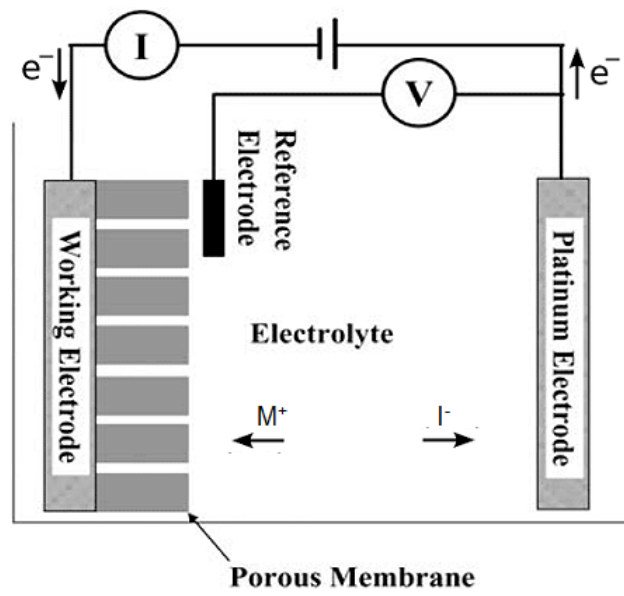


Figure 1.10: Schematic representation of charge flow during templated electrodeposition [20].

Chapter 2

Materials and Methods

The techniques and processes used to synthesize nanowires, induce self-assembly and examine these samples are explained in the following sections.

2.1 Membrane Preparation

Nuclepore Track-Etched (PCTE) membranes with 0.2 μm or 0.05 μm pore diameter were obtained from Whatman. To enable electrodeposition, an electrode was placed on one side of these membranes. In this case, an Au film was sputtered onto the glossy side of the membranes using a Perkin Elmer model 2400 sputtering system. The membranes were placed onto the sample holder and covered with a mask. The background pressure in the chamber was set at $\sim 7.5 \cdot 10^{-7}$ mTorr. Then an Ar atmosphere was created for deposition with a pressure of $2 \cdot 10^{-2}$ mbar. The self bias of the target was set at -600 V and the forward power at 50 W. The deposition was allowed to run for 16 min, which created an Au film of approximately 200 nm thickness.

2.2 Nanowire Synthesis

Various compositions of nanowires were made by templated electrodeposition using an Autolab PGSTAT128N potentiostat/galvanostat from Metrohm Autolab. The membranes with the Au film acted as working electrode, while a small piece of platinum-coated silicon wafer (Pt/Ti/SiO₂/Si) acted as counter electrode. The reference electrode was Ag/AgCl in 3 M KCl (Metrohm Autolab). To ensure deposition only occurred inside the membranes, the backside was first isolated with a small glass plate and teflon tape, so no contact with the electrolyte was possible from this side. Depending on the desired nanowire segments, different electrolyte solutions and voltages were used [21] [22]. Ag segments were made from an aqueous electrolyte containing 0.20 M AgNO₃ (99%, Acros) and 0.10 M H₃BO₃ (99.99%, Sigma-Aldrich), which was adjusted to pH 1.5 using nitric acid (65%, Acros). Depositions were carried out at 0.10 V vs. Ag/AgCl and at room temperature. ZnO segments were deposited from an aqueous electrolyte containing 0.10 M Zn(NO₃)₂·6H₂O (98%, Sigma-Aldrich) at -1.00 V vs. Ag/AgCl and at 60°C. Pt segments were deposited from an

aqueous electrolyte solution containing 0.01 M $\text{H}_2\text{Pt}_2\text{Cl}_6 \cdot 6\text{H}_2\text{O}$ (Sigma-Aldrich) at -0.6 V vs. Ag/AgCl and at room temperature. Au segments were made from an aqueous electrolyte solution containing 0.005 M $\text{HAuCl}_4 \cdot 3\text{H}_2\text{O}$ (99.9%, Sigma-Aldrich) at 0.25 V vs. Ag/AgCl and at room temperature. Finally, segments of p-type Cu_2O were made from an aqueous electrolyte solution containing 0.02 M $\text{CuSO}_4 \cdot 5\text{H}_2\text{O}$ (p.a., BOOM) and 0.34 M lactic acid (88%, Fisher Scientific), which was brought to pH 11 using NaOH (98%, Acros). Depositions took place at -0.4 V vs Ag/AgCl and at 60°C .

After deposition, the membranes were dissolved using CH_2Cl_2 (99.8%, Merck). This solution was washed three times using a Hermle Z36HK centrifuge to separate nanowires from the majority of the solution. After this, CH_2Cl_2 was replaced by either demineralized water for nanoparticle self-assembly or a TE buffer solution for oligomer self-assembly. This whole process is shown schematically in Figure 2.1.

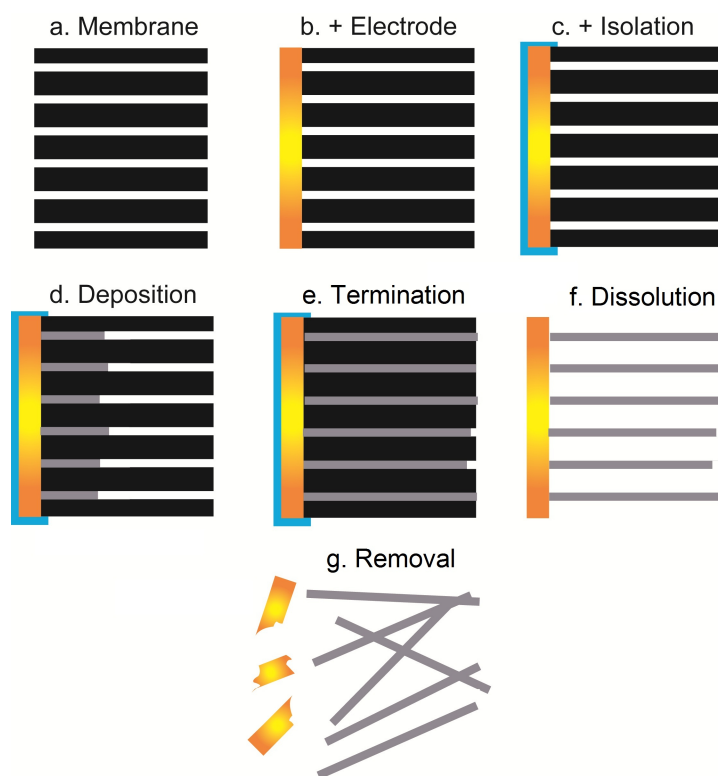


Figure 2.1: Schematic representation of nanowires growth in a membrane during templated electrodeposition.

2.3 Self-Assembly Sample Preparation

Two different types of self-assembly samples were prepared. One set of samples contained nanowires and SiMAG-Thiol nanoparticles from Chemicell GmbH, while another contained nanowires and DNA oligomers. The former were silica nanoparticles with a maghemite core and thiol groups attached to the exterior. A schematic representation of these nanoparticles

is shown in Figure 2.2. Thiol groups have a strong affinity for soft metals like Au, Pt or Ag, which should induce preferential binding to nanowires of these materials.

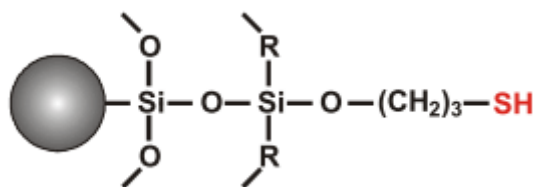


Figure 2.2: Schematic representation of a SiMAG nanoparticle [23].

2.3.1 SiMAG Sample Preparation

The SiMAG self-assembly samples were made in test tubes containing nanowires in demineralized water. 2 μ L of the SiMAG nanoparticles was added to a test tube containing Ag|ZnO nanowires in 6 mL demineralized water. This sample (SiMAG-1-FD) was allowed to self-assemble for one week at 4°C and was then freeze-dried. Next a set of samples was created to examine the effect of time on self-assembly. 2 μ L of SiMAG nanoparticles was added to three identical samples (SiMAG-t1-FD, SiMAG-t2-FD, SiMAG-t3-FD) of Ag|ZnO nanowires in 6 mL demineralized water. One sample was left to self-assemble for 4 days, another one was left for 5 days and the last one was left to self-assemble for 6 days. All of these samples were left at 4°C and subsequently freeze-dried.

The following batch of samples was made to examine the effect of diluting the SiMAG nanoparticles on the self-assembly. This batch was divided into two sub-batches; one was freeze-dried, while the other one was not. All samples were made with Ag|ZnO nanowires. The first one (SiMAG-d1-FD) was made with 6 mL demineralized water containing nanowires and 1 μ L of SiMAG nanoparticles, creating an effective dilution of 6000 \times , corresponding to a SiMAG nanoparticle concentration of 8.3×10^{-3} mg/mL. A sample (SiMAG-d2-FD) with a dilution of 9000 \times , corresponding to a concentration of 5.6×10^{-3} mg/mL, was made by adding 1 μ L of SiMAG nanoparticles to 9 mL of demineralized water containing nanowires. The last sample (SiMAG-d3-FD) was made by adding 0.5 μ L of SiMAG nanoparticles to 6 mL of demineralized water containing nanowires, creating a dilution of 12000 \times , which corresponds to a SiMAG concentration of 4.2×10^{-3} mg/mL. This sub-batch was left to self-assemble at 4°C for approximately 30 hours, after which they were freeze-dried. The same 6000 \times , 9000 \times and 12000 \times dilution samples (SiMAG-d4, SiMAG-d5, SiMAG-d6) were created with the addition of a 3000 \times dilution sample (SiMAG-d7), corresponding to a concentration of 17×10^{-3} mg/mL, by adding 2 μ L of SiMAG nanoparticles to 6 mL of demineralized water containing nanowires. This last sample was created as a reference point and to compare it with a sample made a few months before. This sub-batch was left to self-assemble approximately 24 hours at 4°C as well, but was not freeze-dried.

The final batch of samples was made for analysis with dynamic light scattering (DLS). These samples were made using Au nanowires with a diameter of 50 nm, as opposed to the

previously used nanowires with a diameter of 200 nm. First, a sample (SiMAG-DLS1) was created with a dilution of 1,000,000 \times , which corresponds to a SiMAG concentration of 5×10^{-5} mg/mL, by adding 0.5 μ L of SiMAG nanoparticles to 500 mL of demineralized water containing nanowires. A second sample (SiMAG-DLS2) was created with a dilution of 500,000 \times , which corresponds to a concentration of 1×10^{-4} mg/mL, by adding 0.5 μ L of SiMAG nanoparticles to 250 mL of demineralized water containing nanowires. The third sample (SiMAG-DLS3) was created to achieve a decent count rate required by the DLS machine. This resulted in adding 1.046 μ L of SiMAG nanoparticles to 3 mL of demineralized water containing nanowires, creating an effective dilution of approximately 3000 \times . The final sample (SiMAG-DLS4) of this batch was made by adding 12 drops of a 1,000,000 \times SiMAG particle solution to 3 mL of demineralized water containing nanowires, which created a sample with a SiMAG concentration of approximately 1×10^{-5} mg/mL. The last two samples were monitored by DLS each day for one week.

2.3.2 Oligomer Sample Preparation

Two complementary, thiol-modified DNA oligomer samples were acquired from Eurofins MWG Operon. Strand A contained base sequence CCGCTGTCGTTGCGTGTCTGC, while strand B contained its complement GCAGACACGCAACGACAGCGG. A schematic representation of such an oligomer is shown in Figure 2.3. The idea behind this approach is to fix each strand type to a different nanowire. Subsequently, these are mixed together to allow the complementary strands to pair up, forming a link that effectively attaches two nanowires to each other.

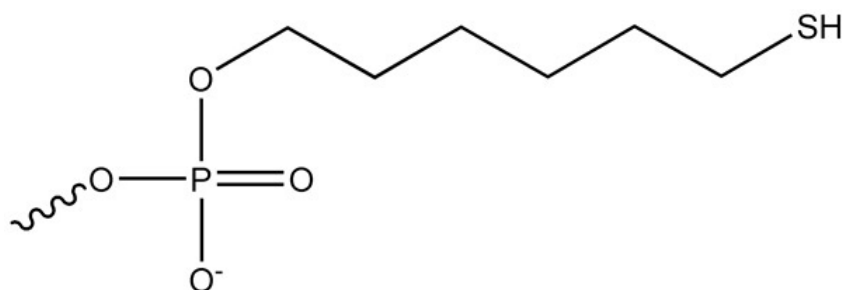


Figure 2.3: Schematic representation of a thiol-modified oligomer. The wavy line symbolizes the actual Watson-Crick base chain [25].

After receipt of the oligomers, reduction of the thiol was necessary before application [24]. For this, 200 μ L 10 mM Tris(2-carboxyethyl)phosphine hydrochloride (TCEP-HCl) (98%, Sigma-Aldrich) was added to each sample, which was then shaken for 60 min at room temperature. The next step was to precipitate the oligomer, which was done by adding 150 μ L 3 M Na-acetate (Sigma-Aldrich). The tube was filled with ethanol and shaken gently. It was left to incubate at -20°C overnight. The next morning, they were centrifuged in a Hermle Z36HK centrifuge at 13000 rpm for 5 min and the supernatant was discarded. The remainder was dried and dissolved in 1.3 mL 10 mM Tris-HCl, 1mM disodium EDTA buffer (TE buffer) solution (Sigma-Aldrich). Both strand batches were split into nine samples of 130 μ L and

frozen at -20°C until further use.

The self-assembly with the oligomers was allowed to take place in test tubes containing the nanowires in TE buffer solution. First, two exploratory samples were created. One sample (Olig1) was made by adding $130\ \mu\text{L}$ of strand A oligomers and $130\ \mu\text{L}$ of strand B oligomers to a test tube containing p-Cu₂O|Au|p-Cu₂O nanowires in 6 mL TE buffer solution. Another (Olig2) was made by adding $130\ \mu\text{L}$ of strand A oligomers and $130\ \mu\text{L}$ of strand B oligomers to a test tube containing Ag|ZnO nanowires in 6 mL TE buffer solution. Both samples were left to self-assemble at 4°C for six days.

Another set of two samples was created in a different fashion. First, $130\ \mu\text{L}$ of strand A oligomer was added to one sample test tube containing Pt|p-Cu₂O nanowires, and another $130\ \mu\text{L}$ to a different test tube containing p-Cu₂O|Au|p-Cu₂O nanowires, both in 4 mL TE buffer solution. The same amount of strand B oligomer was added to two test tubes containing Ag|ZnO nanowires in 4 mL TE buffer solution. These four test tubes were left at 4°C overnight to allow bonding of the oligomers to the nanowires. Afterwards, one sample of Ag|ZnO nanowires with strand B oligomers was added to the Pt|p-Cu₂O nanowires (Olig3) and one Ag|ZnO containing strand B oligomers sample was added to the p-Cu₂O|Au|p-Cu₂O nanowires (Olig4). These remaining two samples were left to self-assemble at 4°C for two days. An overview of all self-assembly samples created in this study is shown in Table 2.1.

2.3.3 Sample Examination

For imaging analysis, small pieces were cut out of a Si wafer and cleaned using ethanol. A few droplets of a sample were deposited onto these small pieces of Si. These Si pieces were then left on a hot plate at 80°C to allow evaporation of the solution. Initially, these Si samples were examined using a Nikon Eclipse ME600 microscope. While nanowires are generally visible under a magnification of 50X/0.80, self-assembly was impossible to determine. For that, the samples were examined using a Zeiss MERLIN scanning electron microscope (SEM). Characterization of nanowires and other objects seen in the SEM was done by energy dispersive x-ray spectroscopy (EDS) using a $80\ \text{mm}^2$ X-Max Silicon Drift Detector from Oxford Instruments.

For DLS analysis, 3 mL of a sample was placed in a cuvette, which was then placed in a Malvern Instruments Zetasizer 3000 HSA particle sizer. Ten subsequent measurements of 120s each were run, each consisting of 10 sub-runs. Two analysis modes were used to examine the data: a contin analysis for samples containing only nanowires or nanoparticles or a non-negative least squares (NNLS) analysis for self-assembly samples. Contin was chosen because it is a relatively simple analysis mode, fit for samples containing one type of particles. The NNLS analysis mode is a high resolution analysis, which is suitable for investigating mixtures of nanoparticles. Additionally, this analysis is more sensitive to the presence of small amounts of material that is larger than the main peak [26].

Sample name	Contents	Self-assembly parameters
SiMAG-1-FD	Ag ZnO nw's and 17×10^{-3} mg/mL SiMAG	7 days at 4°C
SiMAG-t1-FD	Ag ZnO nw's and 17×10^{-3} mg/mL SiMAG	4 days at 4°C
SiMAG-t2-FD	Ag ZnO nw's and 17×10^{-3} mg/mL SiMAG	5 days at 4°C
SiMAG-t3-FD	Ag ZnO nw's and 17×10^{-3} mg/mL SiMAG	6 days at 4°C
SiMAG-d1-FD	Ag ZnO nw's and 8.3×10^{-3} mg/mL SiMAG	30 hours at 4°C
SiMAG-d2-FD	Ag ZnO nw's and 5.6×10^{-3} mg/mL SiMAG	30 hours at 4°C
SiMAG-d3-FD	Ag ZnO nw's and 4.2×10^{-3} mg/mL SiMAG	30 hours at 4°C
SiMAG-d4	Ag ZnO nw's and 8.3×10^{-3} mg/mL SiMAG	24 hours at 4°C
SiMAG-d5	Ag ZnO nw's and 5.6×10^{-3} mg/mL SiMAG	24 hours at 4°C
SiMAG-d6	Ag ZnO nw's and 4.2×10^{-3} mg/mL SiMAG	24 hours at 4°C
SiMAG-d7	Ag ZnO nw's and 17×10^{-3} mg/mL SiMAG	24 hours at 4°C
SiMAG-DLS1	Au nw's and 5×10^{-5} mg/mL SiMAG	1 day at 4°C
SiMAG-DLS2	Au nw's and 1×10^{-4} mg/mL SiMAG	1 day at 4°C
SiMAG-DLS3	Au nw's and approx. 17×10^{-3} mg/mL SiMAG	7 days at 4°C
SiMAG-DLS4	Au nw's and 1×10^{-5} mg/mL SiMAG	7 days at 4°C
Olig1	p-Cu ₂ O Au p-Cu ₂ O nw's in 6 mL TE buffer 130 µL of each A and B	6 days at 4°C
Olig2	Ag ZnO nw's in 6 mL TE buffer 130 µL of each A and B	6 days at 4°C
Olig3	Pt p-Cu ₂ O nw's in 4 mL TE buffer and 130 µL A Ag ZnO in 4 mL TE buffer and 130 µL B	2 days at 4°C
Olig4	p-Cu ₂ O Au p-Cu ₂ O nw's in 4 mL TE buffer and 130 µL A Ag ZnO in 4 mL TE buffer and 130 µL B	2 days at 4°C

Table 2.1: Overview of samples

Chapter 3

Results and Discussion

This chapter shows the results of the experimental work done in this study. First, the SiMAG samples will be discussed. Samples were made to examine freeze-drying, the effect of SiMAG concentration and samples were made for study using dynamic light scattering (DLS). Secondly, the oligomer samples will be discussed.

3.1 Self-Assembly of Nanowires with SiMAG nanoparticles

An initial exploratory self-assembly sample was made with Au nanowires and SiMAG nanoparticles. Figure 3.1 shows clusters of these SiMAG nanoparticles and nanowires. Since no real order was expected for this sample, these clusters were a promising indicator of self-assembly. It could not conclusively be stated that the clusters were formed by self-assembly, as one week is plenty of time for the nanowires and nanoparticles to aggregate by other means, such as diffusion, depletion forces or even plain sedimentation.

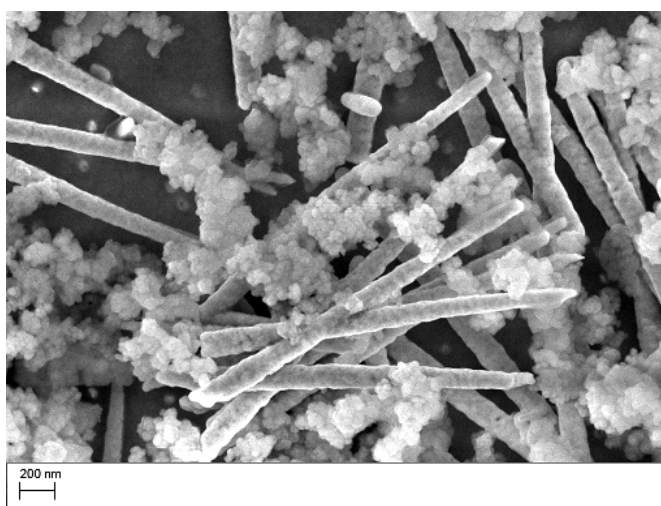


Figure 3.1: SEM image of Au nanowires and SiMAG nanoparticles after self-assembly for approximately one week.

However, there was an inconsistency with the SiMAG nanoparticles that had to be addressed after examining the first sample; drying the nanoparticles at room temperature severely impacted their diameter. According to the supplier, they have a hydrodynamic diameter of approximately 500 nm, which was confirmed with a measurement of the nanoparticles by DLS. However, during drying, the nanoparticles' diameter decreased to approximately 50 nm.

3.1.1 Freeze-Drying

According to the supplier, the shrinking was due to dehydration of the nanoparticles during drying. The carbon chain linking the thiol groups with the silica shell, as can be seen in Figure 2.2, is probably affected. However, it is also unclear what the organic chain denoted by "R" exactly is, so dehydration could also have an effect on those sections. The supplier did not have a suggestion available to prevent dehydration of the nanoparticles, so a method had to be found to prevent this. Initially, critical point drying was proposed to prevent dehydration. However, the satchels in which samples could be enclosed to prevent them from washing away during this process, did not have a small enough mesh to be able to contain the nanowires and nanoparticles. In the end, it was decided to freeze-dry samples to prevent dehydration.

Seven samples were freeze-dried. Despite different self-assembly parameters and SiMAG concentrations, they all showed similar behavior of the SiMAG nanoparticles. A comparison between a sample that was not freeze-dried (a) and a sample that was (b), is shown in Figure 3.2.

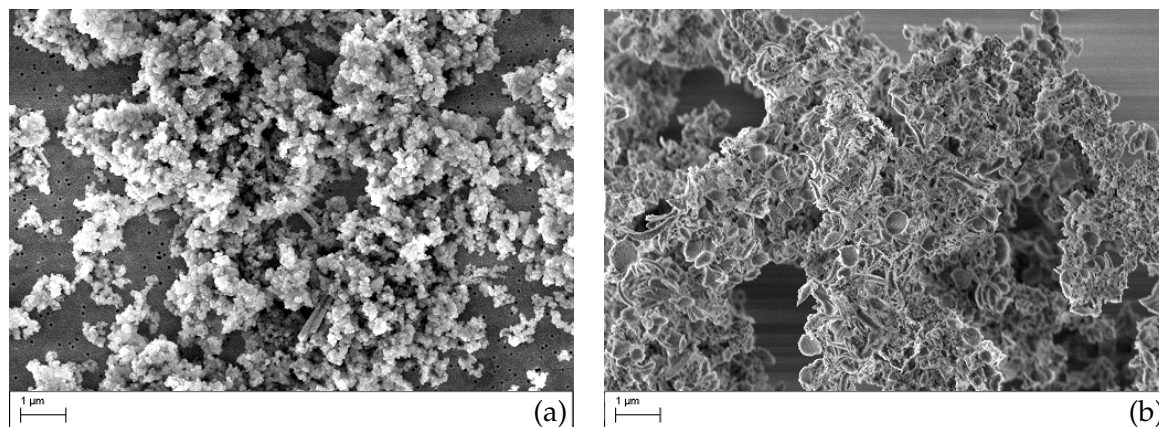


Figure 3.2: Comparison of a non-freeze-dried sample (a) with a freeze-dried sample (b). (a) contains Fe|Pd nanowires and SiMAG nanoparticles after self-assembly for approximately one week, while (b) contains Ag|ZnO nanowires with SiMAG nanoparticles after self-assembly for approximately four days.

While there are several larger circular objects in Figure 3.2b, it is not certain these are SiMAG nanoparticles, since they show little similarity to the surrounding, smaller particles. Most likely, they are organic material. Considering the overall composition of both images is similar, and the fact that all freeze-dried samples looked comparable, it was decided that freeze-drying did not have enough impact to warrant its further use. Especially since it took

more time to be able to analyze freeze-dried samples, as there was always a waiting period to acquire a spot on the machine. This also made samples with regard to self-assembly time difficult to prepare, since it was often unknown when exactly they could be freeze-dried. The overall throughput of freeze-dryer samples was therefore low.

In terms of self-assembly, not much can be said beyond what was already said for the sample in Figure 3.1. Again, large clusters are present. Since these clusters were reproduced, it can be concluded that at least the nanowires and nanoparticles are firmly bonded to each other. There is no order present, but the mechanism proposed for self-assembly seems to work.

3.1.2 The Effect of Self-Assembly Time

Samples that were left to self-assemble for four, five or six days were made to examine the effect of self-assembly time. Figure 3.3 shows SEM images of these samples. A good cluster of SiMAG nanoparticles and nanowires could not be found for the sample left to self-assemble for six days.

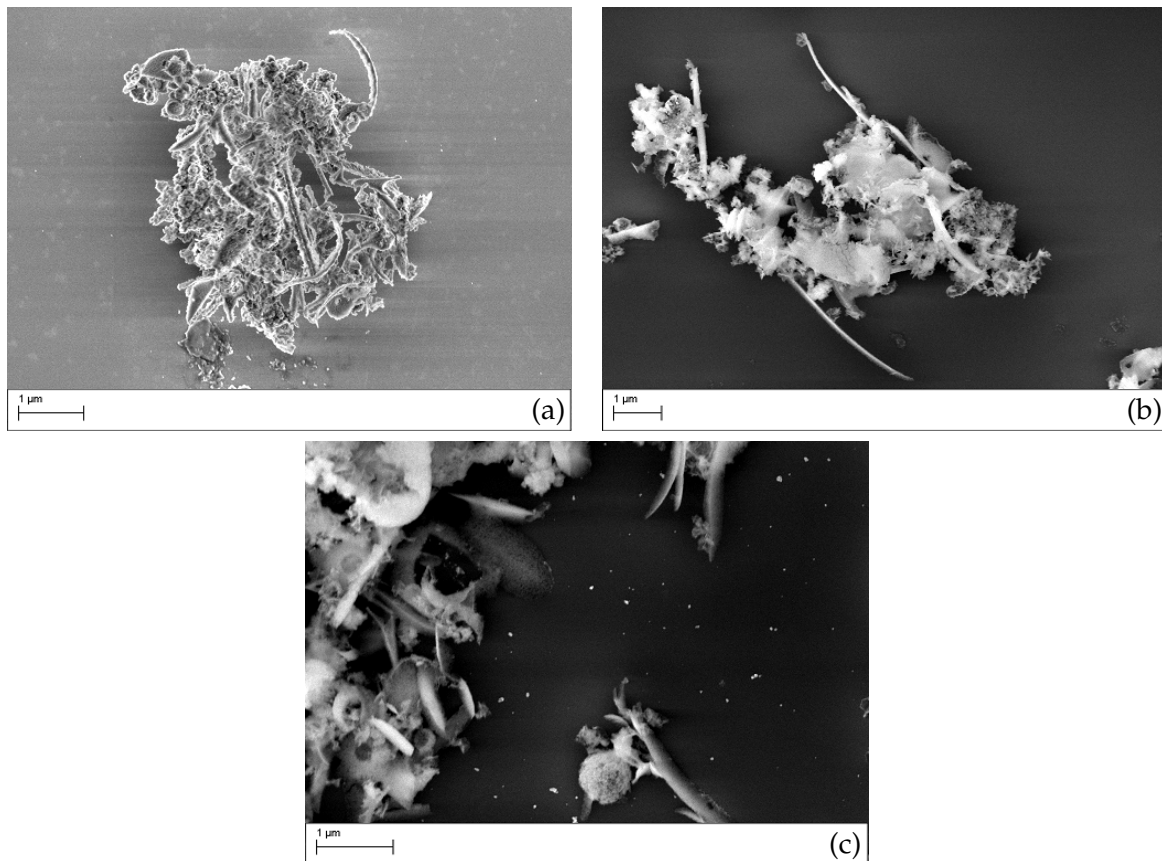


Figure 3.3: SEM images of samples left to self-assemble for four days (a), five days (b) or six days (c). All samples contain Ag | ZnO nanowires with SiMAG nanoparticles.

Both Figure 3.3a and Figure 3.3b show severely deformed nanowires. Most nanowires in all three samples showed some degree of bending, occasionally even forming rings. Additionally, many wires were thinner and longer than they should have been. The reason for these deformations is unclear. It could be due to some effect of the freeze-drying process or some unexpected effect during nanowire synthesis. Since other freeze-drying samples showed no such deformations, it is unlikely freeze-drying is the reason behind the deformations. Despite this, most clusters did show Zn, O, and Fe traces when analyzed by EDS, which points to aggregation of SiMAG nanoparticles and nanowires. Ag was not detected in these clusters. The deposition time for the Ag segments of these wires was low, i.e. 2 seconds. Most likely, not enough Ag was present in the samples to be detected.

Leaving samples for four, five or six days did not have any apparent effect on self-assembly. Four days was already sufficient time to create large clusters. It would be interesting to study the effect of even shorter self-assembly times, in the order of one or two days, or even hours.

3.1.3 The Effect of SiMAG nanoparticle concentration

All previous samples had large amounts of nanoparticles clustered around the nanowires. The SiMAG nanoparticle concentration of previous samples was diluted 3000 \times , yielding a concentration of 17×10^{-3} mg/mL. It was difficult to determine if this clustering occurred because of the desired self-assembly or because of diffusion or some other random effect. Therefore, the next samples (SiMAG-d1 through SiMAG-d7) were made to examine the effect of SiMAG nanoparticle concentration. Samples were made with SiMAG nanoparticle concentrations diluted 6000 \times , 9000 \times and 12000 \times , yielding respective SiMAG concentrations of 8.3×10^{-3} mg/mL, 5.6×10^{-3} mg/mL and 4.2×10^{-3} mg/mL.

As the concentration of SiMAG nanoparticles decreases, the cluster size and quantity decreased as well. However, the number of SiMAG nanoparticles was still very high. Clusters were still relatively large, making it difficult to draw conclusions on self-assembly. Apparently, diluting the SiMAG nanoparticle concentration 12000 \times was not enough. Figure 3.4b shows one of the better clusters, albeit an exceptionally large one. Nanowires are present in abundance. The red arrow points to a larger cluster of SiMAG nanoparticles. The SiMAG nanoparticles are mostly covered by the nanowires in this cluster.

An unexpected effect occurred in samples that were not freeze-dried. Drying of the solution left triangular shapes on the Si, as can be seen in Figure 3.4c. The clusters at the centers of these triangles are shown in Figure 3.4d. Nanowires and SiMAG nanoparticles are present, but they seem to be covered in some kind of organic salt. It is unclear what this is exactly or how it got there.

3.1.4 Self-Assembly Studied by DLS

To investigate the self-assembly without dehydration of the SiMAG nanoparticles, DLS was used to measure the samples in solution. For these samples, Au wires were made, because Au is known to have the best bonding behavior with thiol groups. The concentration of SiMAG nanoparticles was reduced further, as well as the concentration of the nanowires. If both concentrations were very low, any self-assembly would be evident, since aggregation by

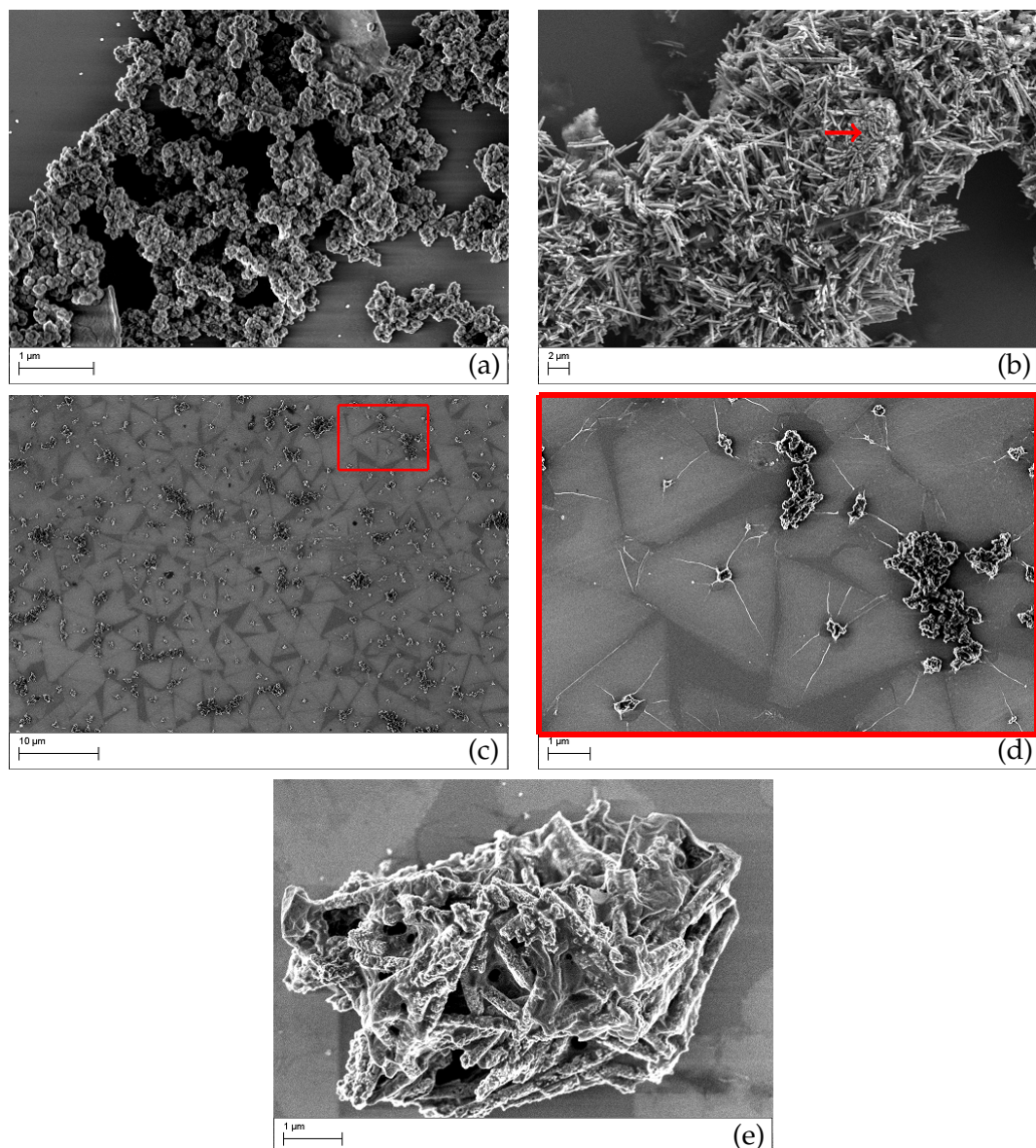


Figure 3.4: SEM images of samples with SiMAG nanoparticle concentrations diluted $3000\times$ (a), $6000\times$ (b) a different $6000\times$ (c), with an enlargement (d), and $12000\times$ (e). All samples contain Ag | ZnO nanowires and were left to self-assemble for approximately one day.

diffusion or depletion forces would be severely limited.

First, SiMAG nanoparticles and nanowires were measured independently to determine a baseline. Graphs of these measurements are shown in Figure 3.5. Each graph denotes one measurement consisting of 10 sub-runs and they show a probability distribution of object sizes. Figure 3.5a shows peaks around 50-100 nm and a broader distribution towards 5000 nm, which respectively correspond to the diameter and length of the nanowires. The SiMAG nanoparticle measurement was done over the course of a few days. Figure 3.5b shows a typical graph of these measurements. Table 3.1 shows the average SiMAG nanoparticle diameters, which are

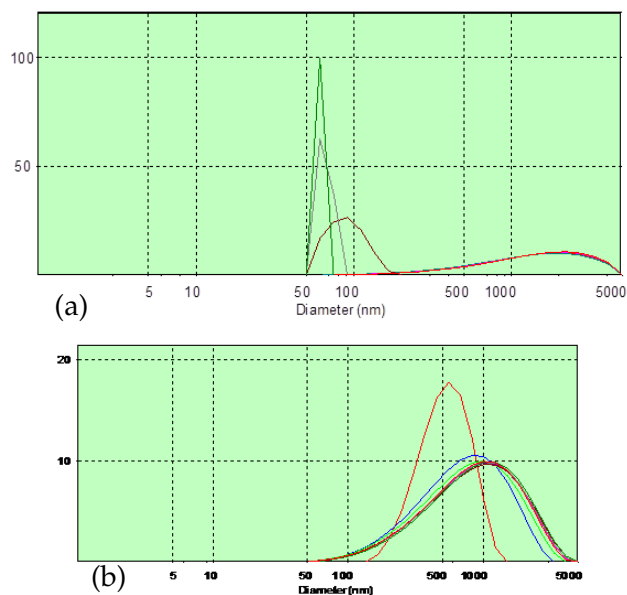


Figure 3.5: (a) DLS graph of 50 nm diameter Au nanowires. (b) DLS graph of SiMAG nanoparticles. The y-axis shows the percentage of objects in a given size distribution.

Self-assembly time (days)	Average diameter (nm)
0	591.8
1	536.9
2	515.7
3	581.9

Table 3.1: SiMAG nanoparticle average diameters.

all in agreement with the hydrodynamic diameter as stated by the supplier.

Samples with the SiMAG particle concentration diluted $1,000,000\times$ (SiMAG-DLS1) and $500,000\times$ (SiMAG-DLS2) were measured by DLS. For a good measurement, the system has to register a minimum of 10 Kcps. Unfortunately, both samples were diluted too much for the system to achieve this lower limit. A new sample (SiMAG-DLS3) was made with a minimum of approximately 10 Kcps. However, to achieve this, the dilution factor was decreased to approximately $3000\times$, which was similar to initial exploratory samples, as well as the samples examining the effect of time of section 3.1.2. Nevertheless, this sample was measured during weekdays over the course of one week. Prior to a measurement, the sample was shaken to break up any clumped up material and to re-suspend the nanowires and SiMAG nanoparticles. The graphs of these measurements are shown in Figure 3.6.

All graphs provide approximately similar diameters. As the self-assembly time increased, the distributions also slightly increased. This could indicate that the object diameters are increasing, implying nanowires and SiMAG nanoparticles are self-assembling. A shift of the graphs along the x-axis, indicating increasing object size, is harder to detect. The average

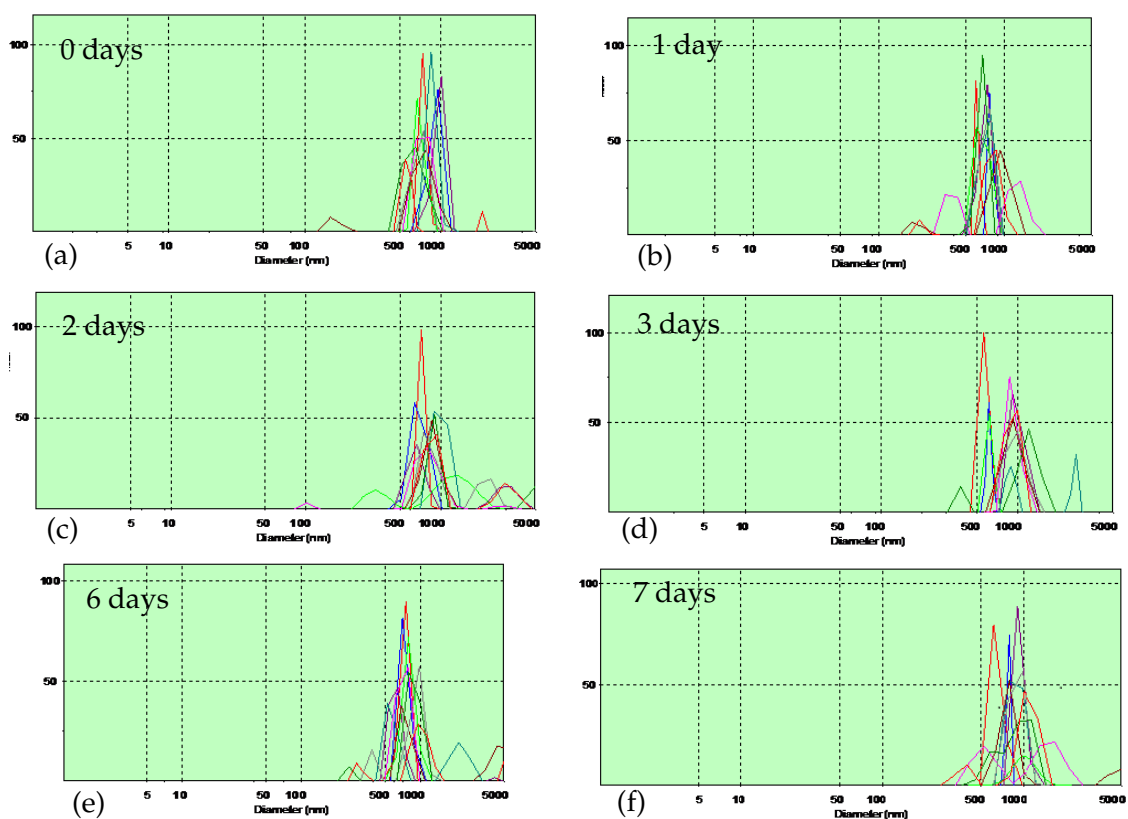


Figure 3.6: DLS graphs of 50 nm diameter Au nanowires and SiMAG nanoparticles diluted approximately $3000\times$. The y-axes show the percentage of objects in a given size distribution.

diameter of each measurement is shown in Table 3.2. The first couple of days showed a clear increase in average object diameter. However, the increase is only about 100 nm. This can be explained by the nanowires bonding to the SiMAG nanoparticles along their length, which would increase the particle diameter by 100 nm, if both sides of the particle have a nanowire bound to it. The graphs do show some small peaks above a diameter of 2000 nm, which could indicate two nanoparticles were linked together by a nanowire. Even with the variety of self-assembled configurations, the fact remains that the average diameter does not increase spontaneously. Therefore, it seems that self-assembly is indeed occurring in this sample.

A final sample (SiMAG-DLS4) was made to study the effect of very dilute SiMAG particle concentration, i.e. 1×10^{-5} mg/mL, even though the concentration was below the minimum required number of counts. The average number of counts of all measurements was 5.3 Kcps. Any results of this sample would be unreliable, so this sample would not contribute to any conclusions about self-assembly. Nevertheless, the effect of a low concentration on a DLS measurement could be investigated. The sample was studied over the course of a week, with measurements done each weekday. The graphs showed individual peaks across the full spectrum of diameters from 5 nm up to 5000 nm. Multiple peaks did seem to occur approximately between the 500 nm and 1000 nm range, which could indicate measurement of SiMAG nanoparticles. The other peaks most likely signify nanowires in several different

Self-assembly time (days)	Average diameter (nm)
0	719.5
1	727.8
2	812.0
3	819.0
6	815.0
7	773.3

Table 3.2: Average object diameters of sample SiMAG-DLS3.

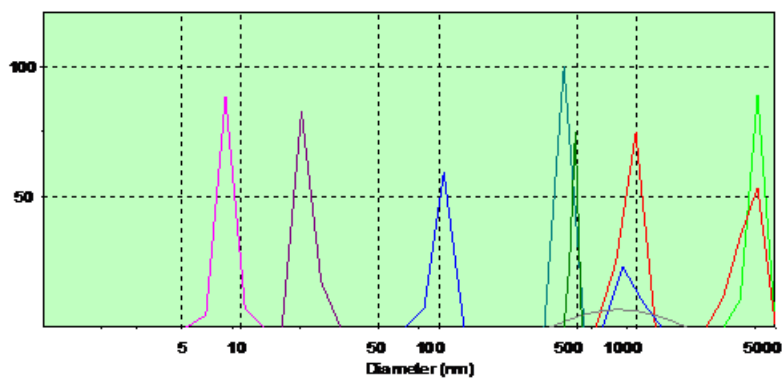


Figure 3.7: Graph of sample SiMAG-DLS4 before self-assembly. The y-axis shows the percentage of objects in a given size distribution.

orientations. A typical graph is shown in Figure 3.7.

The average diameter of each measurement is shown in Table 3.3 and fluctuate largely. The ones below 100 nm are probably measurements of contaminations in the solution instead of nanowires or SiMAG nanoparticles. These averages are low because the solution is too dilute in terms of SiMAG nanoparticles for the DLS system to measure them accurately. No clear conclusions can be drawn on the basis of these averages.

Self-assembly time (days)	Average diameter (nm)
0	237.2
3	55.6
4	214.6
5	140.7
6	77.8

Table 3.3: SiMAG-DLS4 average object diameters.

3.2 Self-Assembly of Nanowires with DNA Oligomers

As stated in the experimental details of section 2.3.2, the oligomers provided by the supplier needed to be reduced before use. However, this procedure did not go as planned. A power outage occurred in the building, which prevented the use of the centrifuge, so the test tubes had to be left in the Na-acetate solution overnight, as opposed to the required 20 min. The following morning, the rest of the procedure was carried out. However, instead of a hard pellet, which was supposed to be found after centrifuging, the substance that remained after discarding the supernatant looked more like a sludge. Additionally, the tube that should have contained the B strands seemed empty. Possibly, the strands were discarded along with the supernatant by mistake. This all meant that the oligomer samples were not very reliable from the start.

Nevertheless, a couple of samples were made, including two exploratory samples (Olig1 and Olig2). Unfortunately, the TE buffer solution that was used to keep the oligomers intact did not dry very well. A substance with high viscosity remained on the Si pieces containing the samples. This made SEM imaging useless, since everything was covered in this residue, as shown in Figure 3.8. Since every sample had this issue, coupled with the fact that the oligomer batches were not very reliable, it was decided to discontinue this part of the study.

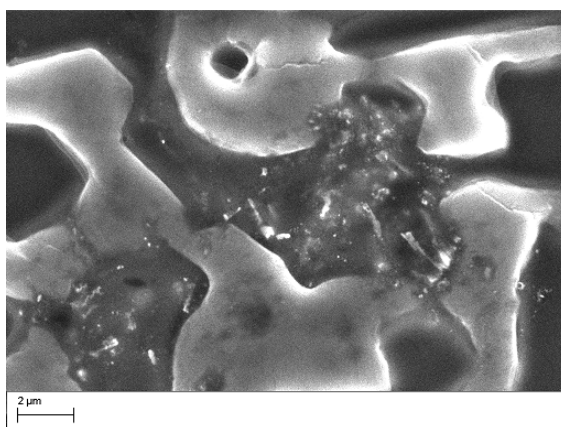


Figure 3.8: SEM image of sample Olig1 showing a possible Ag|ZnO nanowire and SiMAG nanoparticle cluster covered in TE buffer residue.

Conclusions and Recommendations

The goal of this study was to show if it was possible to achieve self-assembly of nanowires. This was investigated by linking nanowires together through thiol-modified DNA oligomers, or by attaching nanowires and thiol-modified SiMAG nanoparticles to each other, which showed some promising results. The aggregates of nanowires and SiMAG nanoparticles seem to have bonded together, indicating that at least the core mechanism works. Furthermore, the results of some of the DLS samples suggest self-assembly occurred. However, it can not be conclusively stated that the aggregates shown in this report are the result of a controlled self-assembly. Furthermore, not all parameters that influence self-assembly could be discovered. Two highly probable main parameters of self-assembly are time and concentration of both SiMAG nanoparticles and nanowires. However, other parameters could be temperature, type of solvent and/or the the stirring of the solvent.

Continuation of this research should be done with Au nanowires exclusively until self-assembly can be achieved reliably. Au interaction with thiol groups is well understood and thiol groups have the highest affinity for Au. While starting with nanowires that have a proven application is admirable, it complicates matters for early research far from the application stage. DLS shows definite promise. Samples in solution do not show shrinkage of the SiMAG nanoparticles that occurred in this study. However, a system that can measure more dilute solutions would be preferable. These very dilute solutions could rule out effects other than desired self-assembly mechanisms. There would be no more need to image each and every sample, which in turn would increase the throughput of samples, eventually allowing more research paths, once self-assembly has actually been proven.

Once self-assembly of nanowires has been proven, it would be interesting to create various superstructures and study the properties of these superstructures or study the effect of these superstructures on material properties. Finding a commercially applicable superstructure would be the next step in this process. Another interesting study would be to find a reversible self-assembly mechanism.

Acknowledgments

I would like to thank several people for their help and guidance during my assignment. Firstly, I would like to thank my daily supervisor Wouter Maijenburg. He was always very helpful and always available to answer any questions I might have or provide his opinion on some strange results I had in the lab.

Next, I would like to thank Marc Ankoné and Mark Smithers. Marc Ankoné handled all the samples that had to be freeze-dried and kept me informed of the machine's availability. Mark Smithers operated the SEM and found the most useful sections of my samples to be imaged.

Finally, I would like to thank the remainder of my graduation committee: André ten Elshof, Gertjan Koster and Michel de Jong. They provided helpful support as well as a promising research avenue at my midterm presentation.

References

- [1] Whitesides, G.M., et al., *Self-Assembly and Nanostructured Materials*. In: Huck, W.T.S., ed., 2005. *Nanoscale Assembly Chemical Techniques*. New York, Springer Science + Business Media, Inc., Ch. 9.
- [2] Nuzzo, R.G., Allara, D.L., 1983. *Adsorption of bifunctional organic disulfides on gold surfaces*. Journal of the American Chemical Society, Vol. 105, Iss. 13, pp. 4481-4483.
- [3] Bain, C.D., et al., 1989. *Formation of Monolayer Films by the Spontaneous Assembly of Organic Thiols from Solution onto Gold*. Journal of the American Chemical Society, Vol. 111, Iss. 1, pp. 321-335.
- [4] Love, J.C., et al., 2005. *Self-Assembled Monolayers of Thiolates on Metals as a Form of Nanotechnology*. Chemical Reviews, Vol. 105, Iss. 4, pp. 1103-1170.
- [5] Anon. *Single Molecule Properties: preparation routes*. Available at: http://www.seas.upenn.edu/~bonnell/research/Single_Molecule_Properties_07_preparation_routes.html, Accessed: 25-06-2013.
- [6] Ramasamy, K., Gupta, A., 2013. *Routes to self-assembly of nanorods*. Journal of Materials Research, Vol. 28, Iss. 13, pp. 1761-1776.
- [7] Ryan, K.M., et al., 2006. *Electric-field-assisted assembly of perpendicularly oriented nanorod superlattices*. Nano Letters, Vol. 6, Iss. 7, pp. 1479-1482.
- [8] Saeedi, E., et al., 2010. *Inertially assisted nanoscale self-assembly*. Nanotechnology, Vol. 21, Iss. 37, p. 375604.
- [9] Smith, B.D., et al., 2011. *Vertical arrays of anisotropic nanoparticles by gravity-driven self-assembly*. Small, Vol. 7, Iss. 6, pp. 781-787.
- [10] Orendorff, C.J., et al., 2005. *pH-Triggered Assembly of Gold Nanorods*. Langmuir, Vol. 21, Iss. 5, pp. 2022-2026.
- [11] Dujardin, E., et al., 2001. *DNA-driven self-assembly of gold nanorods*. Chemical Communications, Iss. 14, pp. 1264-1265.
- [12] Caswell, K.K., et al. 2003. *Preferential end-to-end assembly of gold nanorods by biotin-streptavidin connectors*. Journal of the American Chemical Society, Vol. 125, Iss. 46, pp. 13914-13915.

- [13] Chang, J.Y., et al., 2004. *Oriented assembly of Au nanorods using biorecognition system*. Chemical Communications, Iss. 8, pp. 1092-1094.
- [14] Kim, F., et al. 2001. *Langmuir-Blodgett Nanorod Assembly*. Journal of the American Chemical Society, Vol. 123, Iss. 18, pp. 4360-4361.
- [15] Barano, D., et al., 2010. *Assembly of colloidal semiconductor nanorods in solution by depletion attraction*. Nano Letters, Vol. 10, Iss. 2, pp. 743-749.
- [16] Singh, A., et al., 2012. *Controlled semiconductor nanorod assembly from solution: influence of concentration, charge and solvent nature*. Journal of Materials Chemistry, Vol. 22, Iss. 4, pp. 1562-1569.
- [17] Maijenburg, A.W., 2009. *Master's thesis: Alignment of electrochemically synthesized nanowires*. MSc., University of Twente.
- [18] Bard, A.J., Faulkner, L.R., 2001. *Electrochemical Methods: Fundamentals and Applications*. 2nd Ed. John Wiley & Sons, Inc.
- [19] Henning, T., 2010. *Copper electroplating of a metal (Me) in a copper sulfate bath*. Available at: http://upload.wikimedia.org/wikipedia/commons/thumb/b/b6/Copper_electroplating.svg/1000px-Copper_electroplating.svg.png, Accessed: 28-5-2013.
- [20] Bera, D., et al., 2004. *Synthesis of Nanostructured Materials Using Template-Assisted Electrodeposition*. JOM, Available at: <http://www.tms.org/pubs/journals/JOM/0401/Bera-0401.html>, Accessed: 13-6-2013.
- [21] Maijenburg, A.W., et al., 2011. *Hydrogen Generation from Photocatalytic Silver|Zinc Oxide Nanowires: Towards Multifunctional Multisegmented Nanowire Devices*. Small, Vol. 7, Iss. 19, pp. 2709-2713.
- [22] McShane, C.M., Choi K.S., 2012. *Junction studies on electrochemically fabricated p-n Cu₂O homojunction solar cells for efficiency enhancement*. Physical Chemistry Chemical Physics, Vol. 14, pp. 6112-6118.
- [23] Chemicell, *Product Information - SiMAG-Thiol*. Available at: http://www.chemicell.com/products/microparticles/docs/PI_SiMAG-Thiol_1407.pdf, Accessed: 08-07-2013.
- [24] Eurofins MWG Operon, 2013. *Eurofins MWG Operon - Frequently Asked Questions About Our Products And Services*. Available at: <http://www.eurofinsgenomics.eu/en/eurofins-mwg-operon/product-faqs/dna-rna-oligonucleotides.aspx>, Accessed: 22-5-2013.
- [25] Eurofins MWG Operon, 2013. *Non Fluorescent Modifications & Their Structures*. Available at: <http://www.eurofinsgenomics.eu/en/dna-rna-oligonucleotides/customised-dna-oligos/modified-dna-oligos/non-fluorescent-modifications.aspx>, Accessed: 08-07-2013.
- [26] Malvern Instruments, 2000. *Zetasizer 1000HS/3000HS: Size measurements*. Manual, No. MAN 0149, Iss. 2.0.